



Vapor Equilibrium Data for the Binary Mixtures of Dimethyl Carbonate and Ethyl Methyl Carbonate in Compressed Carbon Dioxide

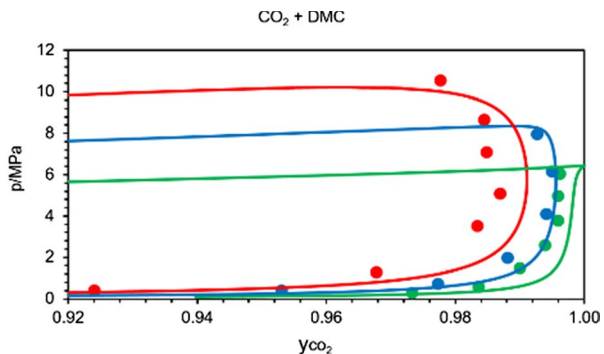
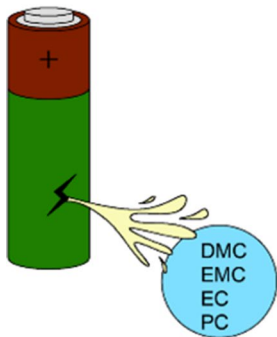
Shiva J. Jethwa^{1,2} · Luis A. Román-Ramírez³ · Paul A. Anderson^{2,4} · Gary A. Leeke^{1,2}

Received: 14 February 2023 / Accepted: 6 March 2023 / Published online: 17 April 2023
© The Author(s) 2023

Abstract

Phase equilibrium data (p , T , y) for the binary systems of carbon dioxide + dimethyl carbonate and carbon dioxide + ethyl methyl carbonate were obtained. All systems were measured for isotherms ranging from 298.2 K to 328.2 K with pressure ranging between 0.13 MPa and 10.6 MPa. A static equilibrium technique was established with samples quantified using an offline method. The results were modeled using the Peng–Robinson equation of state with van der Waals one-fluid mixing rules.

Graphical Abstract



Keywords Electrolyte · Linear carbonates · Lithium-ion batteries · Peng–Robinson equation of state · Solubility · Vapor equilibrium

✉ Gary A. Leeke
g.a.leeke@bham.ac.uk

Extended author information available on the last page of the article

1 Introduction

Carbon dioxide has become an attractive alternative solvent as opposed to traditional organic solvents in recent years, based on its inert, non-toxic, environmentally friendly and non-flammable properties, as well as being relatively inexpensive. Exploring the solute solubility within compressed carbon dioxide for a mixture is a crucial parameter within the field of supercritical practices, allowing the development and optimization of supercritical fluid extraction (SFE) processes [1].

A key component of a lithium-ion battery (LIB) is the non-aqueous electrolyte solution. Currently, many battery recycling techniques are heavily focused on the recovery of valuable metals, with the electrolyte often discarded or combusted during recycling processes. Accounting for 4 % to 8 % of the total cost of the LIB, the electrolyte is one of the least valuable components. Although a minor component of the electrolyte composition is the lithium conducting salt, currently lithium is one of the most valuable raw materials within the LIB, and it has now been classified as a critical material by the European Union [2, 3]. Combined with increasing pressure from battery directives and governmental legislations, the electrolyte is a key component to potentially recycle since it accounts for approximately 10 wt% to 15 wt% of the overall cell [4–7].

The LIB electrolyte is broken down into three main components, solvents, a conducting salt and additives. The bulk volume of the solvents are predominantly constituted of linear carbonates and cyclic carbonates. Linear carbonates, dimethyl carbonate (DMC) and ethyl methyl carbonate (EMC), generally have a lower dielectric constant and are more volatile than their cyclic equivalent, due to their low flash points. Cyclic carbonates, ethylene carbonate (EC) and propylene carbonate (PC), in comparison display higher viscosities and melting points [8, 9].

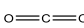
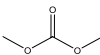
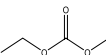
Phase equilibrium data are vital to the design and construction of separation and filtration processes to enable the take up of a supercritical fluid recovery process. The purpose of this research is to obtain comprehensive measurements for the vapor equilibrium of LIB electrolyte in carbon dioxide. Binary mixtures of CO_2 +DMC and CO_2 +EMC were formed at temperatures between 298.2 K and 328.2 K. The experimental data were correlated with the Peng–Robinson equation of state (EoS) and van der Waals (vdW) one-fluid mixing rules. Previously, there have been equilibrium studies of the CO_2 +DMC system with pressure vessels with a magnetic stirrer and circulating-type apparatus. These approaches covered conditions across a limited temperature range of 278 K to 423 K and pressure range of 0.23 MPa to 14.4 MPa [10–13].

The aim of this work was to augment these existing data. A review of the literature revealed that vapor equilibrium data for the CO_2 +EMC system have not been previously published.

Table 1 Chemical specifications

Component name	Molecular formula	CAS	Supplier	Purity (wt%)	Analysis method
Carbon dioxide	CO ₂	124-38-9	BOC UK	> 99.8	
Dimethyl carbonate	(CH ₃ O) ₂ CO	616-38-6	Sigma-Aldrich	> 99.0	GC
Ethyl methyl carbonate	(C ₂ H ₅ O)CO(OCH ₃)	623-53-0	TCI	> 98.0	GC
Acetone	CH ₃ COCH ₃	67-64-1	Fisher Scientific UK	> 99.8	GC

Table 2 Physiochemical properties of compounds

	CO ₂	DMC	EMC
Skeletal structure			
Molar mass (g·mol ⁻¹)	44.009	90.079	104.106
Normal boiling point (K)	194.69	363.11	381.05
Flash point (K)	–	288.15 ^a	296.15 ^a
Critical pressure (MPa)	7.375	4.835	3.839
Critical temperature (K)	304.13	557.38	560.75
Acentric factor (ω)	0.225	0.385	0.429 [*]
Reference	[14]	[15, 16 ^a]	[16 ^a , 17]

*Estimated from: $\omega = -(1/f^1) \left(\text{Ln} \left(\frac{p_c}{1.01315} \right) + f^0 \right)$, where f^0 and f^1 are Ambrose–Walton parameters for vapor pressure estimation and p_c is the critical pressure [18]

2 Experimental Section

2.1 Materials and Reagents

The chemicals used in the experimental work are presented in Table 1. All chemicals were used without further purification and were verified via gas chromatographic (GC) analysis, to exhibit equal or greater chemical assay than that provided by suppliers. Table 2 outlines the physiochemical properties of CO₂, DMC and EMC.

2.2 Experimental Apparatus and Methods

The solubility measurements were performed in a Baskerville BS5500 pressure vessel (W015198, Baskerville R&A, Cast P6625), with a design pressure of 33.1 MPa up to 403.15 K. The vessel was equipped with three sapphire windows and a heating jacket. The pressure was recorded with a transducer (Druck PTX 1400) that was connected to an indicator (Druck DPI), displaying readings accurate up to 0.01 MPa. The heating jacket was maintained using a Polyscience

circulator (model-9505), and the temperature of the vessel was recorded using a K-type thermocouple connected to a temperature readout (TME Electronics), providing readings accurate to 0.1 K. A gas chromatograph (GC) equipped with a thermal conductivity detector (GC-TCD) (Thermo Science Trace 1300) was used to quantify samples offline. GC-TCD data were interpreted using a Chromeleon 7 chromatography data system. The GC-TCD used helium as the carrier gas, with a certified purity of 99.996 % obtained from BOC. Separation of the components was carried out in a 30 m×0.25 mm fused silica (Rxi-35Sil MS) column. The sampling loop was assembled using three Swagelok ball valves (SS-41GS1), a Hoke micro-metering valve (1315G2Y) and Swagelok tubing (OD 1/16 in., wall thickness 0.02 in.), and the assembly is displayed in Fig. 1.

Prior to collecting the vapor samples, the internal volume of the sampling loop was measured. The preliminary volume was estimated using the manufacturing specifications from the valves and tubing instrumentation. A more precise method involved filling the entire sampling loop with DMC and then flushing the loop with acetone repeatedly until the DMC gave no detectable GC signal. An average sampling loop volume was found to be 0.104 ± 0.009 mL, taken from a range of 10 samples. The relative standard deviation (RSD) in this value was calculated as 5.02 %. The sample solution was prepared to a volume of 10 mL with acetone before injecting the sample into the gas chromatograph. Repeats were conducted after the sampling loop was washed with 30 mL of acetone to remove any DMC traces.

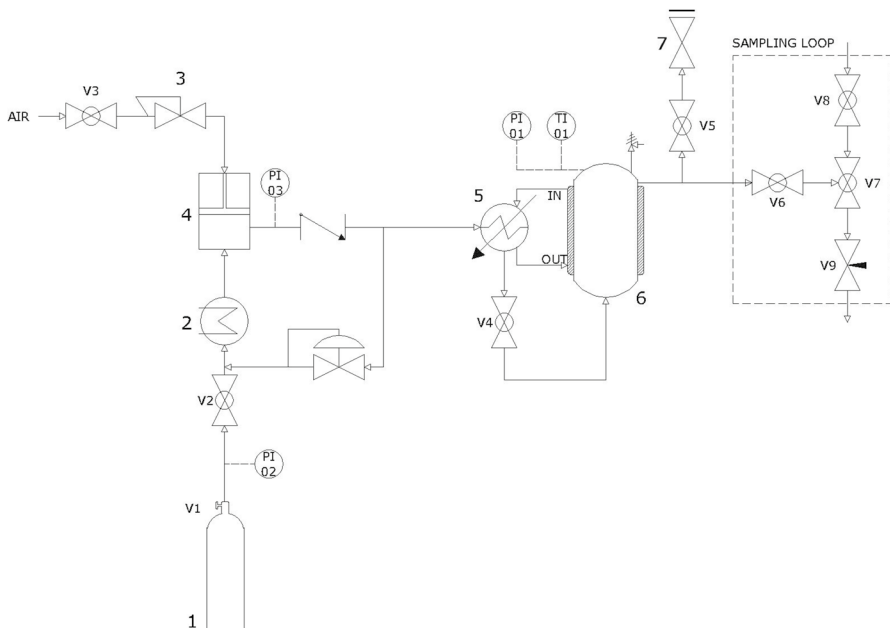


Fig. 1 Schematic of the high-pressure solubility rig: (1) CO₂ gas canister; (2) sub-zero glycol bath; (3) air regulator; (4) gas booster; (5) hot water bath; (6) pressure vessel; (7) outlet vent. *PI* pressure indicator, *TI* temperature indicator

2.3 Procedure

Solubility data of $\text{CO}_2 + \text{DMC}$ and $\text{CO}_2 + \text{EMC}$ were collected over a temperature range of 298.2 K to 328.2 K and a pressure range of 0.13 MPa to 10.6 MPa. A 15-mL sample of the DMC and EMC sample was placed within the vessel, sealed and then purged with carbon dioxide for 5 min at a constant flow to displace any air present within the vessel. The desired temperature was then set, and the vessel contents were left to reach equilibrium for a minimum of 8 h. This time was deemed sufficient as GC analysis showed no significant change in the solubility beyond this interval. Once equilibrium was achieved, three samples were taken consecutively to clear the lines between the reactor and sampling loop, and a vapor sample was then collected through the sampling loop and gradually bubbled through ice-cooled acetone via the metering valve, allowing the carbon dioxide to escape while trapping the solvent within the solution. Once the vapor sample had been completely expanded, the sampling loop was washed with excess acetone to capture any DMC or EMC sample residue. Next, the sampling loop was washed with acetone, left to dry and vacuumed, ready for the next vapor sample. The solution of either the DMC or EMC sample and acetone was then injected into the gas chromatograph and quantified using calibration curves for each solute. The coefficient of determination (R^2) was 0.9991 for DMC and 0.9998 for EMC. The vapor mole fraction and solubility of the solute were calculated using the following equations:

$$y_{\text{CO}_2} = \frac{n_{\text{CO}_2}}{n_{\text{total}}}, \quad (1)$$

$$n_{\text{solute}} = \frac{(\rho_{\text{solute}} \cdot V_{\text{solute}})}{M_{\text{r solute}}}, \quad (2)$$

$$n_{\text{CO}_2} = \frac{(\rho_{\text{CO}_2} \cdot (V_{\text{sampleloop}} - V_{\text{solute}}))}{M_{\text{r CO}_2}}, \quad (3)$$

$$S_{\text{solute}} = \frac{m_{\text{solute}}}{m_{\text{CO}_2}}, \quad (4)$$

$$= \frac{(\rho_{\text{solute}} \cdot V_{\text{solute}})}{(\rho_{\text{CO}_2} \cdot (V_{\text{sampleloop}} - V_{\text{solute}}))}, \quad (5)$$

where n are the number of moles of the solvent/solute component, ρ represents the associated density ($\text{kg} \cdot \text{m}^{-3}$), V is the volume (m^3), M_{r} represents the molar mass of the substance ($\text{g} \cdot \text{mol}^{-1}$) and m is the mass of the solvent/solute component (g).

2.4 Modeling

In addition, the experimental data for both systems were correlated against the Peng–Robinson EoS (Eq. 6) with the vdW one-fluid mixing rules. Equation 8 is the recently updated version of the generalized Soave α -function [19].

$$p = \frac{RT}{V-b} - \frac{a(T)}{V(V+b) + b(V-b)}, \quad (6)$$

$$a(T) = 0.45724 \frac{R^2 T_c^2}{p_c} \left\{ 1 + k \left[1 - \left(\frac{T}{T_c} \right)^{0.5} \right] \right\}^2, \quad (7)$$

$$k = 0.3919 + 1.4996\omega - 0.2721\omega^2 + 0.1063\omega^3, \quad (8)$$

$$b = 0.07780 \frac{RT_c}{p_c}, \quad (9)$$

$$a_m = \sum_i \sum_j x_i x_j a_{ij}, \quad (10)$$

$$b_m = \sum_i x_i b_i, \quad (11)$$

$$a_{ij} = (1 - k_{ij}) a_i^{0.5} a_j^{0.5}, \quad (12)$$

where p is the pressure (MPa), R defines the molar gas constant ($\text{J}\cdot\text{mol}^{-1}\cdot\text{K}^{-1}$), T is the absolute temperature (K), T_c is the critical temperature (K), V is the molar volume ($\text{m}^3\cdot\text{mol}^{-1}$), k_{ij} represents the binary interaction parameter, the parameter a is a function of temperature and parameter b is a constant.

The optimum k_{ij} was regressed from the experimental pressures (p_{exp}) and the CO_2 vapor compositions ($y_{\text{CO}_2,\text{exp}}$) according to the objective function F given by Eq. 13. N_p in Eq. 13 stands for the number of data points used in the fitting, and PR stands for a calculated property with the PR EoS. Phase diagrams from the obtained k_{ij} were produced by the isothermal flash algorithm.

$$F = \sum_{i=1}^{N_p} \left[\left(\frac{p_{\text{exp},i} - p_{\text{PR},i}}{p_{\text{exp},i}} \right)^2 + (y_{\text{CO}_2,\text{exp},i} - y_{\text{CO}_2,\text{PR},i})^2 \right]. \quad (13)$$

3 Results and Discussion

The experimental data points for both binary systems, CO₂ + DMC and CO₂ + EMC, are presented in Tables 3 and 4, respectively, where the mole fraction of carbon dioxide in the vapor phase is represented by y_{CO_2} , and the solubility of each solute in carbon dioxide is represented by S . The standard deviation (SD) is outlined for both solubility and mole fraction measurements to capture the associated variance in the data.

The modeling results are presented in Table 5. The estimated optimum binary interaction parameter was $k_{ij} = -0.02$ for both systems.

Relative percentage deviation for pressure ($\% \Delta p$) and for CO₂ vapor mole fraction ($\% \Delta y_{\text{CO}_2}$) was computed from Eqs. 14 and 15, respectively.

$$\% \Delta p = \left| \frac{(p_{\text{exp}} - p_{\text{PR}})}{p_{\text{exp}}} \right| \times 100, \quad (14)$$

$$\% \Delta y_{\text{CO}_2} = \left| \frac{(y_{\text{CO}_2, \text{exp}} - y_{\text{CO}_2, \text{PR}})}{y_{\text{CO}_2, \text{exp}}} \right| \times 100. \quad (15)$$

Table 3 Experimental values of vapor mole fraction y , and solubility S at temperature T , and pressure p , for the binary system, CO₂ + DMC^a

T (K)	p (MPa)	S_{EMC} (g·g ⁻¹)	S_{DMC} SD	y_{CO_2}	y_{CO_2} SD
298.2	0.32	0.0566	0.00373	0.9731	0.00172
	0.61	0.0343	0.00341	0.9835	0.00161
	1.5	0.0210	0.00343	0.9899	0.00164
	2.6	0.0128	0.00284	0.9938	0.00137
	3.8	0.0087	0.00081	0.9958	0.00039
	5.0	0.0087	0.00094	0.9958	0.00046
313.2	6.1	0.0045	0.00077	0.9961	0.00037
	0.42	0.1010	0.01081	0.9530	0.00481
	0.75	0.0475	0.00442	0.9773	0.00207
	2.0	0.0250	0.00624	0.9880	0.00173
	4.1	0.0124	0.00276	0.9940	0.00133
	6.2	0.0105	0.00344	0.9949	0.00166
328.2	8.0	0.0202	0.00143	0.9926	0.00069
	0.41	0.1689	0.01809	0.9239	0.00754
	1.3	0.0683	0.00879	0.9677	0.00402
	3.5	0.0349	0.00180	0.9833	0.00085
	5.1	0.0273	0.00144	0.9868	0.00069
	7.1	0.0315	0.00260	0.9848	0.00123
	8.7	0.0324	0.00166	0.9844	0.00078
	10.6	0.0467	0.00576	0.9777	0.00268

^aStandard uncertainties are $u(T)=0.1$ K, $u(p)=0.01$ MPa, $u(y_{\text{CO}_2})=0.008$

Table 4 Experimental values of vapor mole fraction y , and solubility S at temperature T , and pressure p , for the binary system, $\text{CO}_2 + \text{EMC}^a$

T (K)	p (MPa)	S_{EMC} ($\text{g}\cdot\text{g}^{-1}$)	S_{EMC} SD	y_{CO_2}	y_{CO_2} SD
298.2	0.13	0.0373	0.00412	0.9845	0.00169
	0.63	0.0180	0.00338	0.9925	0.00141
	1.0	0.0042	0.00254	0.9966	0.00058
	1.8	0.0023	0.00032	0.9975	0.00034
	3.5	0.0028	0.00142	0.9981	0.00053
	5.7	0.0023	0.00061	0.9985	0.00039
	7.8	0.0016	0.00033	0.9989	0.00046
313.2	0.41	0.0550	0.00417	0.9773	0.00168
	0.74	0.0244	0.00304	0.9898	0.00126
	2.1	0.0114	0.00242	0.9952	0.00101
	3.3	0.0055	0.00019	0.9977	0.00008
	5.2	0.0032	0.00104	0.9987	0.00044
	7.3	0.0098	0.00035	0.9959	0.00015
	328.2	0.17	0.1364	0.01111	0.9478
0.98		0.0446	0.00624	0.9811	0.00254
2.8		0.0172	0.00680	0.9928	0.00162
5.5		0.0137	0.00551	0.9943	0.00231
8.1		0.0294	0.00167	0.9877	0.00056
9.6		0.0453	0.00364	0.9812	0.00148

^aStandard uncertainties are $u(T)=0.1$ K, $u(p)=0.01$ MPa, $u(y_{\text{CO}_2})=0.005$

Table 5 Modeled vapor mole fraction y as a function of temperature T , and pressure p for the binary systems, $\text{CO}_2 + \text{DMC}$ and $\text{CO}_2 + \text{EMC}$ using the PR EoS

T (K)	$\text{CO}_2 + \text{DMC}$				$\text{CO}_2 + \text{EMC}$			
	p (MPa)	y_{CO_2}	$\% \Delta p$	$\% \Delta y_{\text{CO}_2}$	p (MPa)	y_{CO_2}	$\% \Delta p$	$\% \Delta y_{\text{CO}_2}$
298.2	0.33	0.9820	1.873	0.915	0.13	0.9742	2.174	1.046
	0.61	0.9901	0.284	0.671	0.65	0.9946	2.831	0.212
	1.5	0.9956	0.998	0.576	1.0	0.9964	1.984	0.020
	2.6	0.9972	0.283	0.342	1.8	0.9977	0.982	0.020
	3.8	0.9979	0.240	0.211	3.5	0.9986	0.355	0.050
	5.0	0.9983	0.736	0.251	5.7	0.9991	0.356	0.060
	6.1	0.9990	0.680	0.291				
313.2	0.43	0.9705	2.548	1.836	0.44	0.9830	5.434	0.583
	0.74	0.9823	1.086	0.512	0.73	0.9892	1.454	0.061
	2.0	0.9925	1.516	0.455	2.1	0.9954	1.336	0.020
	4.1	0.9952	0.791	0.121	3.3	0.9965	1.031	0.120
	6.2	0.9955	0.473	0.060	5.2	0.9969	0.732	0.180
	8.0	0.9941	0.000	0.151	7.3	0.9964	0.104	0.050
328.2	0.40	0.9380	2.829	1.526	0.15	0.9014	12.709	4.896
	1.3	0.9785	2.211	1.116	1.0	0.9834	1.613	0.234
	3.5	0.9896	1.293	0.641	2.8	0.9922	0.554	0.060
	5.1	0.9910	0.696	0.426	5.5	0.9937	0.495	0.060
	7.2	0.9906	0.909	0.589	8.2	0.9918	0.840	0.415
	8.7	0.9882	0.478	0.386	9.6	0.9869	0.360	0.581

Experimental data obtained for the $\text{CO}_2 + \text{DMC}$ system were compared with the literature data as presented in Fig. 2. The literature data were taken from: Lee *et al.* (293.15 K, 303.15 K, 313.15 K, 323.15 K and 333.15 K), Im *et al.* (310.27 K and 330.3 K) and Li *et al.* (333.0 K). The literature data collected for comparative studies adopted two types of experimental methods, both Im *et al.* and Lee *et al.* applied a circulating-type apparatus, and Li *et al.* used a high-pressure cell with a magnetic stirrer. In comparison with the static setup adopted, both literature experimental methods implemented better fluid circulation of the two components, though in our research this was alleviated by increasing the duration to reach vapor–liquid equilibrium.

As observed in Fig. 2, an exact comparison could not be made between the experimental and literature data at temperatures of 298.2 K and 328.2 K. However, the experimental data at 298.2 K fit within the isotherms of 293.15 K and 303.15 K from Lee *et al.* denoting good agreement. Similarly, the experimental data at 328.2 K hold a close fit to both datasets obtained from Lee *et al.* (333.15 K) and Im *et al.* (330.3 K). The largest RSD across all isotherms for y_{CO_2} was calculated to be 0.816 %.

A review of literature data revealed no vapor–liquid equilibrium work has been performed for the second binary system, $\text{CO}_2 + \text{EMC}$; for this reason, the

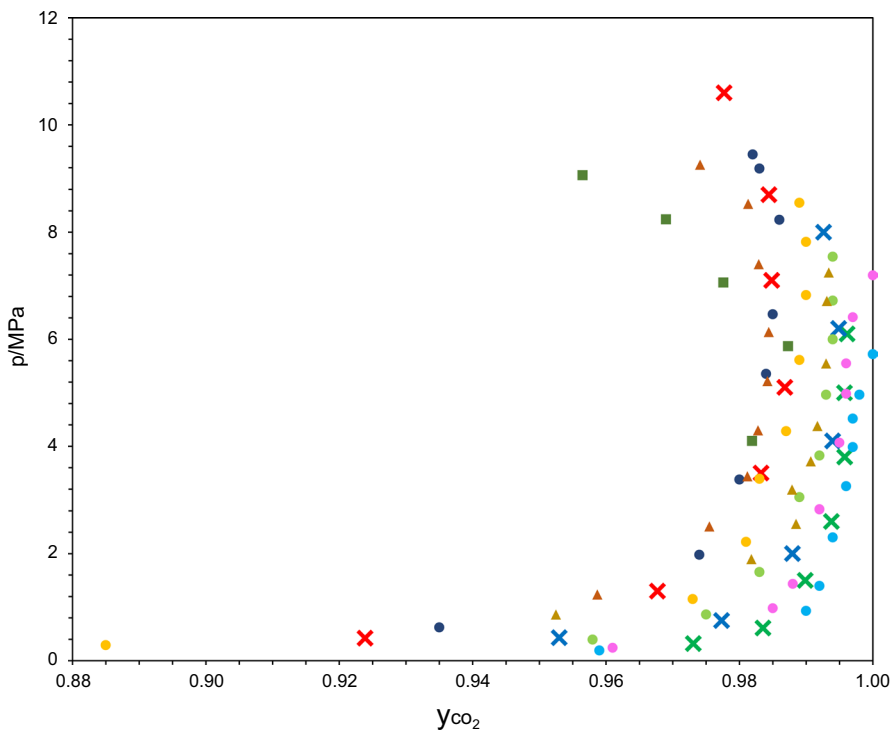


Fig. 2 Experimental phase equilibrium data of the $\text{CO}_2 + \text{DMC}$ binary system. This work: (x) 298.2 K, (x) 313.2 K, (x) 328.2 K. Lee *et al.*: (●) 293.15 K, (●) 303.15 K, (●) 313.15 K, (●) 323.15 K, (●) 333.15 K. Im *et al.*: (▲) 310.27 K, (▲) 330.3 K. Li *et al.*: (■) 333.0 K [10–12]

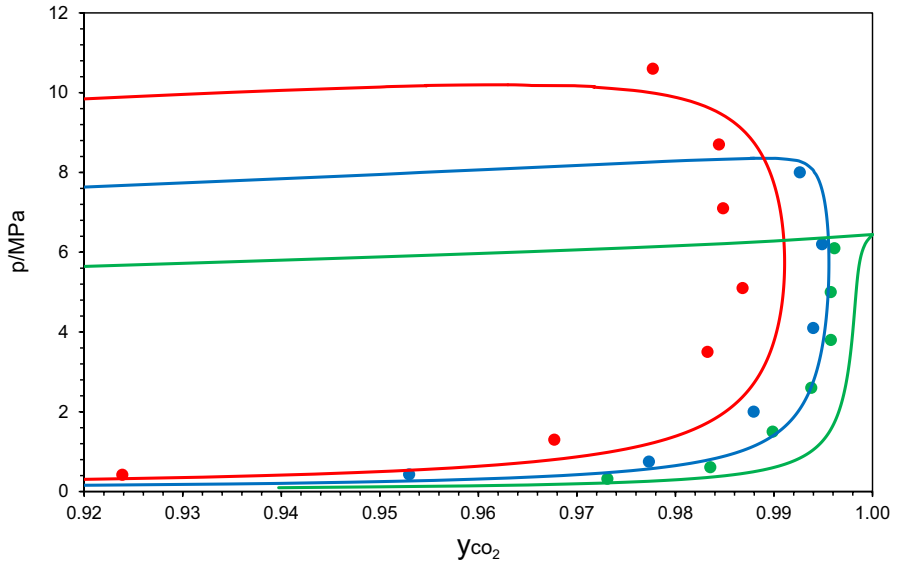


Fig. 3 Phase diagram for the $\text{CO}_2 + \text{DMC}$ binary system. Experimental data (●) 298.2 K, (●) 313.2 K, (●) 328.2 K, (—) PR EoS

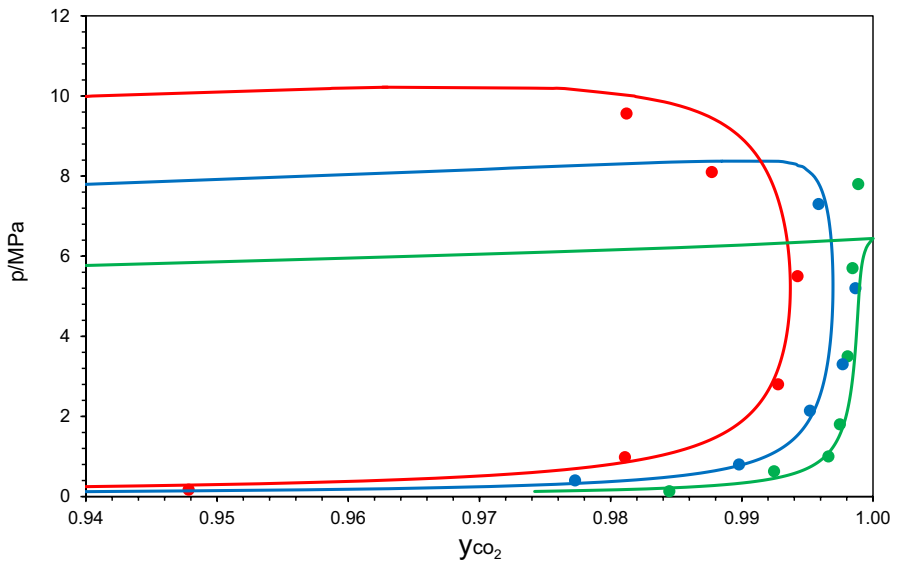


Fig. 4 Phase diagram for the $\text{CO}_2 + \text{EMC}$ binary system. Experimental data (●) 298.2 K, (●) 313.2 K, (●) 328.2 K, (—) PR EoS

experimental data could not be compared against any literature work, though to verify the consistency and fit, the data were modeled against the PR EoS, as

presented in Fig. 4. The maximum RSD found for y_{CO_2} in this system was calculated to be 0.442 %.

The two carbonate components are observed in Figs. 3 and 4 to each exhibit high solubilities in carbon dioxide at low pressure isothermally, resulting in a decrease in vapor phase densities and an increase in densities in the liquid phase. In isobaric state, a high solubility of components in carbon dioxide is experienced as the absolute temperature increases, and this is a consequence of the increasing vapor pressure of the solute and decrease in densities in the vapor phase.

Overall, the deviation between the $\text{CO}_2 + \text{DMC}$ experimental and modeled data across all isotherms was comparatively low; the maximum relative percentage deviation of p and y_{CO_2} was calculated as 2.83 % and 1.84 %, respectively. Similarly, a comparison of both experimental and modeled data for the $\text{CO}_2 + \text{EMC}$ system confirmed a good fit across all isotherms; the upmost relative percentage deviation of P and y_{CO_2} was calculated as 12.71 % and 4.90 %, respectively.

4 Conclusion

The vapor phase equilibrium data were measured at three temperatures, 298.2 K, 313.2 K and 328.2 K, at pressures ranging from 0.13 MPa to 10.6 MPa. The data were modeled using the Peng–Robinson (EoS) using the updated version of the generalized Soave α -function and the vdW one-fluid mixing rules. Satisfactory agreement between experimental and modeled phase equilibrium data was obtained. The largest RSD across all isotherms for both $\text{CO}_2 + \text{DMC}$ and $\text{CO}_2 + \text{EMC}$ binary systems was 0.816 % and 1.94 %, respectively.

Author Contributions SJ was involved in experiment and writing—original draft; LR was involved in data modeling and writing—review and editing; PA was involved in writing—review and editing; and GL was involved in supervision, writing—review and editing and project management.

Funding The authors would like to acknowledge funding from the Faraday Institution through the Recycling of Lithium-Ion Batteries (ReLiB) Project: (FIRG005, FIRG027 and FIRG057).

Data Availability The data that support the findings of this study are available from the corresponding author upon reasonable request.

Declarations

Conflict of interest The authors have no competing interests as defined by Springer, or other interests that might be perceived to influence the results and/or discussion reported in this paper.

Ethical Approval Not applicable.

Open Access This article is licensed under a Creative Commons Attribution 4.0 International License, which permits use, sharing, adaptation, distribution and reproduction in any medium or format, as long as you give appropriate credit to the original author(s) and the source, provide a link to the Creative Commons licence, and indicate if changes were made. The images or other third party material in this article are included in the article's Creative Commons licence, unless indicated otherwise in a credit line to the material. If material is not included in the article's Creative Commons licence and your intended use is

not permitted by statutory regulation or exceeds the permitted use, you will need to obtain permission directly from the copyright holder. To view a copy of this licence, visit <http://creativecommons.org/licenses/by/4.0/>.

References

1. Q. Li, P. Pan, T. Lu, S. Blackburn, G.A. Leeke, J. Chem. Eng. Data **64**, 9 (2018). <https://doi.org/10.1021/acs.jced.8b00388>
2. X. Lin, X. Wang, G. Liu, G. Zhang, *Recycling of Power Lithium-Ion Batteries: Technology, Equipment, and Policies* (Wiley, New York, 2022), pp.23–25
3. European Commission, *Critical Raw Materials Resilience: Charting a Path towards greater Security and Sustainability* (European Commission, 2020), p. 24
4. J.B. Dunn, L. Gaines, M. Barnes, M.Q. Wang, J. Sullivan, *Material and Energy Flows in the Materials Production, Assembly, and End-of-Life Stages of the Automotive Lithium-Ion Battery Life Cycle*, Department of Energy (Lemont, Argonne National Laboratory, 2012), pp. 2–10
5. P. Ribière, S. Grugeon, M. Morcrette, S. Boyanov, S. Laruelle, G. Marlair, Energy Environ. Sci. **5**, 5271 (2012). <https://doi.org/10.1039/C1EE02218K>
6. Y. Liu, D. Mu, R. Zheng, C. Dai, RSC Adv. **4**, 54525 (2014). <https://doi.org/10.1039/C4RA10530C>
7. A. Sattar, D. Greenwood, M. Dowson, P. Unadkat, *Automotive Lithium ion Battery Recycling in the UK* (International Manufacturing Centre (WGM), Warwick University, 2020), pp. 1–12
8. J.T. Warner, *Lithium-Ion Battery Chemistries* (Elsevier, Amsterdam, 2019), pp. 141–152
9. Q. Li, J. Chen, L. Fan, X. Kong, Y. Lu, Green Energy Environ. **1**, 18 (2016). <https://doi.org/10.1016/j.gee.2016.04.006>
10. J. Im, M. Kim, J. Lee, H. Kim, J. Chem. Eng. Data **49**, 243 (2004). <https://doi.org/10.1021/je034089a>
11. M.H. Lee, J.-H. Yim, J.W. Kang, J.S. Lim, Fluid Phase Equilib. **318**, 77 (2012). <https://doi.org/10.1016/j.fluid.2012.01.020>
12. L. Chen, R.-J. Zhu, P.-F. Yuan, L.-Q. Cao, Y.-L. Tian, Acta Phys. Chim. Sin. **29**, 11 (2013). <https://doi.org/10.3866/pku.Whxb201210262>
13. R.P. Ciccolini, A.C. Madlinger, S.A. Rogers, J.W. Tester, J. Chem. Eng. Data **55**, 2673 (2010). <https://doi.org/10.1021/je900948n>
14. *Compound Summary for CID 280, Carbon dioxide* (National Library of Medicine, PubChem, 2022)
15. C.L. Yaws, *Yaws' Critical Property Data for Chemical Engineers and Chemists* (Knovel, New York, 2012)
16. J. Ma, *Battery Technologies: Materials and Components* (Wiley-VCH, Weinheim, 2021), pp.21–22
17. X. Zhang, J. Zuo, C. Jian, J. Chem. Eng. Data **55**, 4896 (2010). <https://doi.org/10.1021/je100494z>
18. B.E. Poling, J.M. Prausnitz, J.P. O'Connell, *Properties of Gases and Liquids*, 5th edn. (McGraw-Hill Education, New York, 2001)
19. A. Pina-Martínez, R. Privat, J.-N. Jaubert, D.-Y. Peng, Fluid Phase Equilib. **485**, 264 (2019). <https://doi.org/10.1016/j.fluid.2018.12.007>

Publisher's Note Springer Nature remains neutral with regard to jurisdictional claims in published maps and institutional affiliations.

Authors and Affiliations

Shiva J. Jethwa^{1,2} · Luis A. Román-Ramírez³ · Paul A. Anderson^{2,4} · Gary A. Leeke^{1,2}

¹ School of Chemical Engineering, University of Birmingham, Birmingham B15 2TT, UK

² The Faraday Institution, Quad One, Harwell Science and Innovation Campus, Didcot OX11 0RA, UK

- ³ Division of Chemical and Energy Engineering, School of Engineering, London South Bank University, 103 Borough Road, London SE1 0AA, UK
- ⁴ School of Chemistry, University of Birmingham, Birmingham B15 2TT, UK